# Separable roles for *Mycobacterium tuberculosis* ESX-3 effectors in iron acquisition and virulence

JoAnn M. Tufariello[a,b], Jessica R. Chapman[c], Christopher A. Kerantzas[a], Ka-Wing Wong[d], Catherine Vilchèze[a,e], Christopher M. Jones[f], Laura E. Cole[a], Emir Tinaztepe[g], Victor Thompson[g], David Fenyö[h,i], Michael Niederweis[f], Beatrix Ueberheide[c,i], Jennifer A. Philips[g,1,2,3], and William R. Jacobs Jr.[a,e,2,3]

[a]Department of Microbiology and Immunology, Albert Einstein College of Medicine, Bronx, NY 10461; [b]Department of Medicine, Albert Einstein College of Medicine, Bronx, NY 10461; [c]Office of Collaborative Science, New York University School of Medicine, New York, NY 10016; [d]Shanghai Public Health Clinical Center, Key Laboratory of Medical Molecular Virology of the Ministry of Education/Health, School of Basic Medical Sciences, Fudan University, Shanghai 201508, China; [e]Howard Hughes Medical Institute, Albert Einstein College of Medicine, Bronx, NY 10461; [f]Department of Microbiology, University of Alabama at Birmingham, Birmingham, AL 35294; [g]Division of Infectious Diseases, Department of Medicine, New York University School of Medicine, New York, NY 10016; [h]Laboratory of Computational Proteomics, Center for Health Informatics and Bioinformatics, New York University School of Medicine, New York, NY 10016; and [i]Department of Biochemistry and Molecular Pharmacology, New York University School of Medicine, New York, NY 10016

Contributed by William R. Jacobs Jr., December 4, 2015 (sent for review September 19, 2015; reviewed by Sarah M. Fortune and Celia W. Goulding)

***Mycobacterium tuberculosis*** **(Mtb) encodes five type VII secretion systems (T7SS), designated ESX-1–ESX-5, that are critical for growth and pathogenesis. The best characterized is ESX-1, which profoundly impacts host cell interactions. In contrast, the ESX-3 T7SS is implicated in metal homeostasis, but efforts to define its function have been limited by an inability to recover deletion mutants. We overcame this impediment using medium supplemented with various iron complexes to recover mutants with deletions encompassing select genes within *esx-3* or the entire operon. The *esx-3* mutants were defective in uptake of siderophore-bound iron and dramatically accumulated cell-associated mycobactin siderophores. Proteomic analyses of culture filtrate revealed that secretion of EsxG and EsxH was codependent and that EsxG–EsxH also facilitated secretion of several members of the proline-glutamic acid (PE) and proline-proline-glutamic acid (PPE) protein families (named for conserved PE and PPE N-terminal motifs). Substrates that depended on EsxG–EsxH for secretion included PE5, encoded within the *esx-3* locus, and the evolutionarily related PE15–PPE20 encoded outside the *esx-3* locus. In vivo characterization of the mutants unexpectedly showed that the ESX-3 secretion system plays both iron-dependent and -independent roles in Mtb pathogenesis. PE5–PPE4 was found to be critical for the siderophore-mediated iron-acquisition functions of ESX-3. The importance of this iron-acquisition function was dependent upon host genotype, suggesting a role for ESX-3 secretion in counteracting host defense mechanisms that restrict iron availability. Further, we demonstrate that the ESX-3 T7SS secretes certain effectors that are important for iron uptake while additional secreted effectors modulate virulence in an iron-independent fashion.**

*Mycobacterium tuberculosis* | type VII secretion system | ESX-3 | mycobactin | siderophore

Bacterial secretion systems play roles in pathogenesis, antigenicity, and virulence and are keys to understanding host–pathogen interactions (1, 2). *Mycobacterium tuberculosis* (Mtb), the causative agent of tuberculosis (TB), encodes five type VII secretion systems (T7SS) within genomic loci referred to as "*esx-1*" through "*esx-5*" (3). There is considerable interest in understanding these secretion systems, because they appear to be central to Mtb pathogenesis. ESX-1 has been studied most extensively because deletion of a large portion of this coding region is the primary attenuating mutation in *Mycobacterium bovis-bacillus Calmette–Guérin* (bacillus Calmette–Guérin), the widely used TB vaccine (4–6). In addition to containing the secretion apparatus itself, *esx-1* encodes several substrates, including a pair of small helical proteins belonging to the WXG100 family as well as members of the proline-glutamic acid (PE) and proline-proline-glutamic acid (PPE) families (named for conserved N-terminal amino acid signatures) (7). A large body of data points to the importance of ESX-1 in modulating host cell signaling and bacterial trafficking, perhaps in large measure because of a membrane-lytic function (8, 9). However, the precise mechanisms whereby individual substrates contribute to ESX-1 functions are less clear. The less-investigated ESX-3 provides an alternate system by which we can explore how T7SS contribute to growth and virulence. ESX-3 has been thought primarily to play a bacterial intrinsic role in metal homeostasis. This notion is based on the observation that the *esx-3* gene cluster (*Rv0282–Rv0292*) is transcriptionally de-repressed in response to iron and zinc starvation and on genetic data pointing to a role for ESX-3 in using iron bound to the siderophore mycobactin (Mb) in both nonpathogenic mycobacteria and Mtb (10–13). Similar to the *esx-1* locus, *esx-3* also encodes a pair of WXG100 family members (EsxG and EsxH) and PE–PPE proteins (PE5 and PPE4) (3), but their specific functions remain largely undefined.

Emerging data point to additional roles of ESX-3 in virulence and modulation of immune responses. Introduction of Mtb *esx-3* into *Mycobacterium smegmatis* (Msmeg) strains lacking the

## Significance

***Mycobacterium tuberculosis*** **(Mtb) uses type VII secretion systems to secrete cognate protein pairs that alter host interactions. Here, we address the contributions of the ESX-3 secretion system to Mtb growth and pathogenesis through a combination of genetics, proteomics, and growth studies both in vitro and in vivo. ESX-3 is demonstrated to play a critical role in iron acquisition through secretion of a pair pf proteins belonging to the PE–PPE family (PE5–PPE4). In vivo, the importance of PE5–PPE4 secretion was found to depend upon host genotype, likely reflecting a host capacity to restrict iron availability. However, secreted effectors EsxG–EsxH play an iron-independent role in Mtb virulence. Therefore, ESX-3 secretes multiple effectors that target distinct host pathways to influence pathogenesis.**

Author contributions: J.M.T., C.A.K., K.-W.W., C.V., C.M.J., M.N., B.U., J.A.P., and W.R.J. designed research; J.M.T., J.R.C., C.A.K., K.-W.W., C.V., C.M.J., L.E.C., E.T., and V.T. performed research; J.M.T., J.R.C., C.A.K., K.-W.W., C.V., C.M.J., L.E.C., E.T., D.F., M.N., B.U., J.A.P., and W.R.J. analyzed data; and J.M.T., J.R.C., C.A.K., B.U., J.A.P., and W.R.J. wrote the paper.

Reviewers: S.M.F., Harvard School of Public Health; and C.W.G., University of California, Irvine.

The authors declare no conflict of interest.

[1]Present address: Division of Infectious Diseases, Department of Medicine, Washington University School of Medicine, St. Louis, MO 63110.

[2]J.A.P. and W.R.J. contributed equally to this work.

[3]To whom correspondence may be addressed. Email: jphilips@dom.wustl.edu or jacobsw@hhmi.org.

This article contains supporting information online at www.pnas.org/lookup/suppl/doi:10.1073/pnas.1523321113/-/DCSupplemental.

endogenous locus generates altered cytokine responses, and, when used as a vaccine, this strain protects against subsequent challenge with Mtb (14). EsxG and EsxH form a heterodimer (15) and generate prominent CD4 and CD8 T-cell responses in mice and humans (16–18). The EsxG–EsxH complex impairs phagosomal maturation by interfering with the host endosomal sorting complex required for transport (ESCRT) (19). Finally, repression of the entire *esx-3* locus in bacillus Calmette–Guérin impairs bacterial survival in macrophages (13). Although ESX-3 has been implicated in both metal homeostasis and virulence, it is not known whether these two phenomena are related, and the roles of specific effectors are undefined. Investigation of these questions has been hampered by the essentiality of ESX-3 in standard laboratory medium. Here, we isolated Mtb strains lacking ESX-3 and mutants deficient in the secreted substrates EsxG, EsxH, and PE5–PPE4 by recovering the strains on iron-supplemented media. We evaluated the *esx-3* region mutants with regard to their iron and zinc phenotypes, their ability to produce mycobactin, their capacity for siderophore-mediated iron uptake, and their virulence in macrophages and in mice. Further, by comparing culture filtrates (CFs) of WT and knockout strains using label-free quantitative MS, we comprehensively defined ESX-3–secreted factors and determined their codependence on EsxG and EsxH. By comparing the phenotypic data with the secretome analysis, we were able to link secretion of particular substrates to specific effector functions. The phenotypic and proteomic analyses point to a model in which PE5 and PPE4 are the critical ESX-3 substrates involved in metal homeostasis and in counteracting host iron restriction, while EsxG and EsxH also play an essential iron-independent role in virulence.

## Results

**Hemin and Mb Rescue Growth of Mtb Δ*esx-3*, Δ*esxG*, Δ*esxH*, and Δ*pe5–ppe4*.** Because ESX-3 has been implicated in using Mb-bound iron (13), we reasoned that we might be able to recover mutants in the *esx-3* locus if we used hemin as an alternative iron source (20, 21). Because Esx proteins and PE–PPE family members are implicated as substrates of T7SS (7, 22), we generated strains lacking *esxG*, *esxH*, and *pe5–ppe4*, all of which are encoded within *esx-3* (Fig. S1 *A* and *G–I*, Table S1, and Dataset S1), as well as a complete *esx-3* deletion (i.e., Δ*Rv0282–Rv0292*) (Fig. S1 *A–F*) and, for comparison of iron phenotypes, a deletion mutant of *mbtB* (Fig. S1*J*), which codes for a peptide synthase required to produce Mb (23) (see *SI Materials and Methods* for details of iron-containing media used to recover mutants). The Δ*esx-3* mutant, Δ*esxG*, Δ*esxH*, the double-knockout Δ*pe5–ppe4*, and Δ*mbtB* all grew on medium containing 100 μM hemin, failed to grow on unsupplemented medium (Fig. 1 *A* and *B*), and were rescued with integrating plasmids expressing the relevant genes under control of the heat-shock protein 60 (*hsp60*) promoter (Fig. S2*A* and Table S2) or, for Δ*esx-3* and Δ*mbtB*, with a cosmid containing the entire *esx-3* region or the entire *mbt-1* Mb synthesis locus, respectively (Fig. 1 *A* and *B*, Fig. S2*A*, and Table S2). For unclear reasons, Δ*esx-3*, Δ*esxH*, and Δ*pe5–ppe4* also required Tween 80 to grow on hemin-containing medium, whereas Δ*esxG* and Δ*mbtB* did not (Fig. 1*A*).

Previous work in Msmeg suggested that ESX-3 participates in the utilization of iron bound to Mb (13). Therefore, we were surprised at the abundant growth of Mtb Δ*esx-3* when 2 μg/mL mycobactin J (MbJ) (a standard concentration used for culturing *Mycobacterium avium* subsp. *paratuberculosis*) was provided. On titrating MbJ, we found that 100-fold more MbJ was needed for growth rescue of the *esx-3* mutants than for growth rescue of the Δ*mbtB* mutant (Fig. 1*B*). Similarly, 10-fold more hemin was needed to rescue Δ*esxH* than to rescue Δ*mbtB* (Fig. 1*A* and Fig. S2*B*), and most of the mutants were not effectively rescued by supplementation with an approximately sixfold excess of ferric ammonium citrate (FAC) and a 10-fold excess of zinc sulfate (Fig. S2*C*), compared with standard 7H10 medium. The only exception was Δ*esxG*, which grew with zinc supplementation and was further

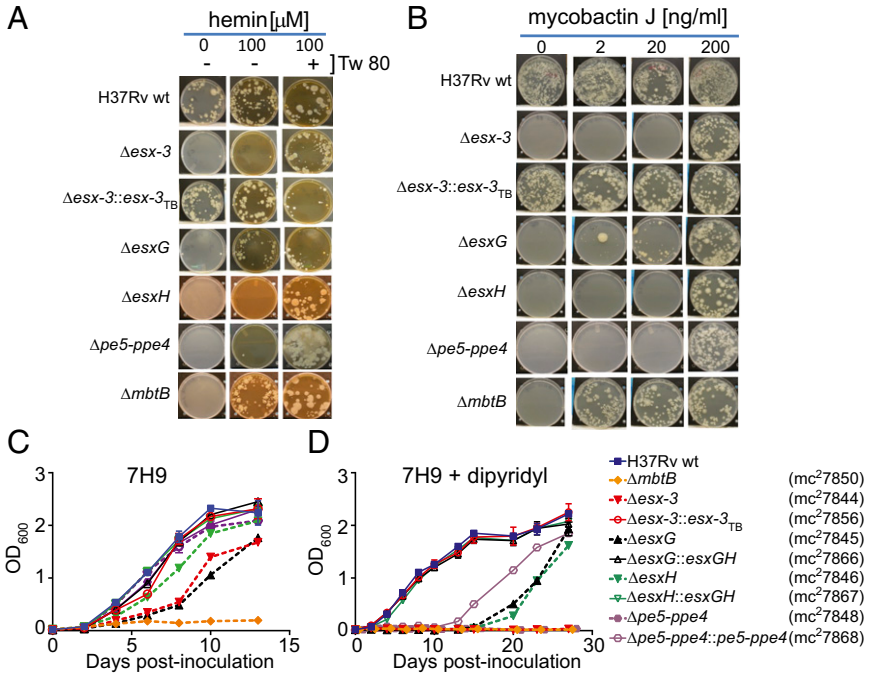


**Fig. 1.** Defined iron sources rescue the essentiality of *esx-3* region mutants. (*A* and *B*) The indicated Mtb strains H37Rv WT, Δ*esx-3* (mc$^2$7788), Δ*esx-3*::*esx-3*$_{TB}$ (mc$^2$7827), Δ*esxG* (mc$^2$7789), Δ*esxH* (mc$^2$7790), Δ*pe5–ppe4* (mc$^2$7792), and Δ*mbtB* (mc$^2$7808) (Fig. S1 and Table S1) were plated on 7H10 medium with or without 100 μM hemin and Tween 80 (0.05%) (Tw 80) (*A*) or with increasing concentrations of MbJ (*B*). Some late-appearing contamination was present when Δ*pe5–ppe4* was plated on medium containing hemin and Tween 80 in *A*. (*C* and *D*) The indicated strains, which differ from those used in the plating experiments shown in *A* and *B* in that the *sacB-hyg*$^R$ cassettes were removed, were grown in 7H9 medium (*C*) or 7H9 medium supplemented with 100 μM 2,2′-dipyridyl (*D*). Data points represent the mean ± SEM from duplicate cultures.

enhanced by additional FAC after prolonged incubation (Fig. S2 *C* and *D*). Thus, Δ*esxH* and Δ*pe5–ppe4* phenocopy Δ*esx-3*, but Δ*esxG* exhibits a somewhat distinct phenotype. In contrast to the findings on solid medium, the *esx-3* mutants had relatively mild growth defects in 7H9 broth unless the lipophilic iron chelator 2,2′-dipyridyl was included (Fig. 1 *C* and *D*), but growth of Δ*mbtB* was severely restricted even in nonchelated medium (Fig. 1*C*). In conclusion, the data are consistent with *esx-3* playing a role in siderophore-mediated iron acquisition, a role that appears to be more crucial on solid medium than in liquid medium. Furthermore, ESX-3 is nonessential provided that iron is available in an accessible form. This result suggests the presence of a less efficient uptake system(s) that functions in the absence of ESX-3. Finally, the high concentration of hemin required to rescue growth of the *esx-3* region mutants suggests potential involvement of ESX-3 in iron uptake from other sources in addition to siderophores.

**The *esx-3* Mutants Overproduce Mb and Fail to Assimilate Mb-Bound Iron.** When grown in iron-replete 7H9 broth, the *esx-3* region mutants developed a distinct orange pigmentation (Fig. S3*A*), which we reasoned might represent excess Mb. To address this possibility, bacteria were grown under iron-limited conditions (chelated Sauton's medium) in the presence of 7-[$^{14}$C]-salicylic acid, the biosynthetic precursor of Mb. These experiments used *esx-3* and *mbtB* mutants generated in the auxotrophic mc$^2$6230 (H37Rv Δ*RD1* Δ*panCD*) strain background (Table S1), which facilitates work with radiolabeled, infectious samples because it can be used at biosafety level 2 (BSL2) (24, 25). When analyzed by TLC, only Mb was observed in cell pellets, whereas the CF contained both Mb and carboxymycobactin (cMb). Δ*mbtB* showed the expected absence of Mb and cMb (26, 27). In contrast, Δ*esx-3* produced Mb slightly in excess of the parental strain, which was restored to WT levels in the complemented strain (Fig. S3*B*). When cell pellet extracts from Δ*esx-3*, Δ*esxG*, Δ*esxH*, and Δ*pe5–ppe4* grown in iron-replete 7H9 medium were analyzed by TLC, the orange-pigmented material comigrated with Mb; this material was undetectable in H37Rv WT, Δ*esx-3*::*esx-3*$_{TB}$, and Δ*mbtB* (Fig. S3*C*). These data are consistent with the idea that the *esx-3* mutants experience iron deprivation in standard 7H9 medium and respond by up-regulating production of Mb. In iron-limited medium, both WT and *esx-3* region mutants experience iron starvation and increase production of Mb, so the differential increase for the mutants is less apparent. To quantify the relative accumulation of Mb in the Δ*esx*-3 and Δ*esxH* mutant strains, we analyzed them by MS after growth in 7H9 as described in *SI Materials and Methods*. As expected, Mb and cMb were absent or were present in trace amounts in extracts of the Δ*mbtB* strain (Fig. 2*A*). In the Δ*esx*-3 and Δ*esxH* strains there was >15-fold accumulation of Mb in the cell pellets and CF compared with the parental strain, accounting for >4% of total lipids in both fractions. cMb also was increased in the CF of the mutants, although the changes were more modest (Fig. 2*A*).

Because a previously described Δ*mmpS4/S5* siderophore export mutant became "intoxicated" by excess intracellular siderophores (28), we asked whether the Mb accumulation in the mutants might contribute to their growth defect. We deleted the entire *mbt-1* gene cluster in strains lacking both *esxG* and *esxH* or *esx-3* (Fig. S1 *K* and *L*) and found that the Δ*esxG–esxH* Δ*mbt-1* double-deletion strain behaved similarly to Δ*esxG–esxH* in requiring high concentrations (200 ng/mL) of MbJ for growth on solid medium (Fig. 2*B*). Similarly, the Δ*esx-3* Δ*mbt-1* double

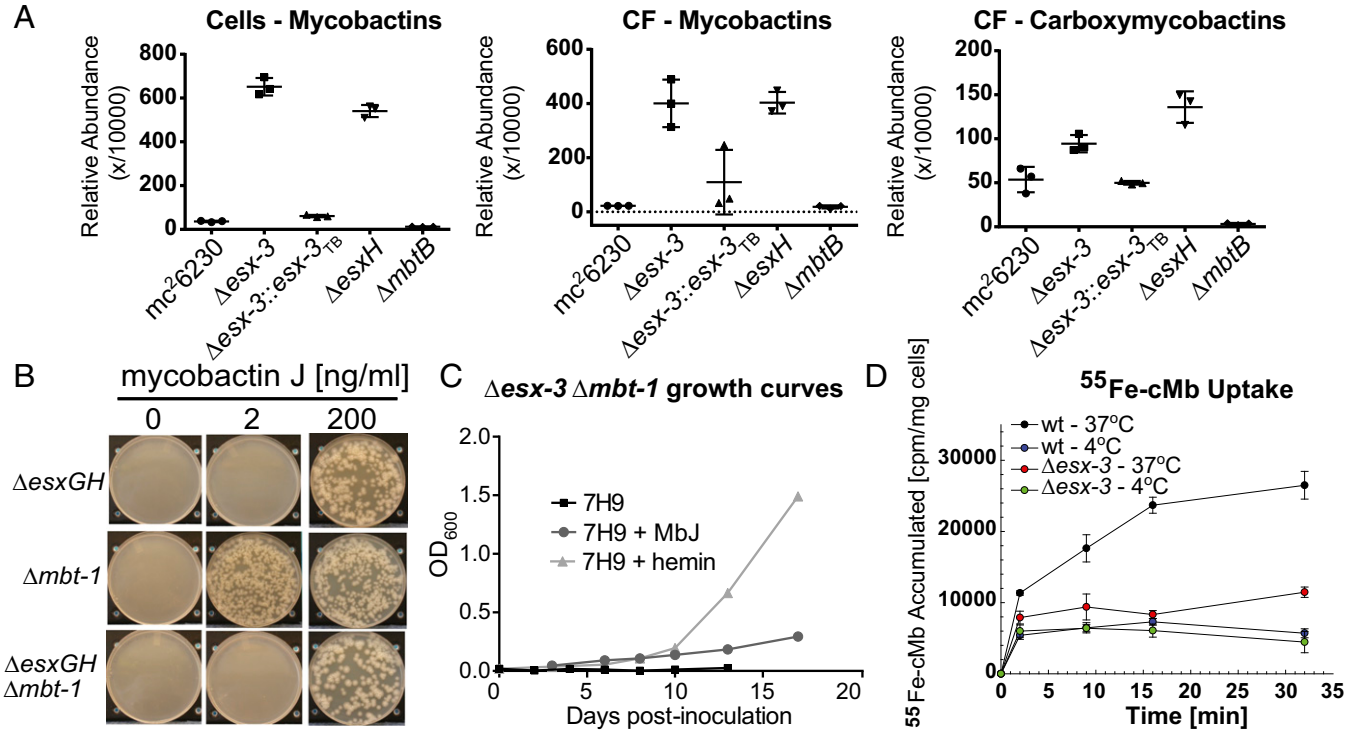


**Fig. 2.** *esx-3* region mutants produce Mb but fail to assimilate Mb-bound iron. (*A*) UPLC-MS analysis of lipids extracted from WT (mc$^2$6230) and the indicated mutant strains [Δ*esx-3* (mc$^2$7860), Δ*esx3*::*esx-3*$_{TB}$ (mc$^2$7863), Δ*esxH* (mc$^2$7861), and Δ*mbtB* (mc$^2$7862)] following growth in 7H9 medium without Tween 80 for 3 wk. The amount of Mb and cMb was normalized to total lipids in each sample and reported as a relative abundance out of 10,000 arbitrary units. Data points show the values for individual samples; lines indicate mean ± SD. (*B*) Δ*esxG–esxH* (mc$^2$7791), Δ*mbt-1* (mc$^2$7809), and Δ*esxG–esxH* Δ*mbt-1* (mc$^2$7851) were grown on 7H10 medium containing MbJ as indicated. (*C*) The Δ*esx3* Δ*mbt-1* double mutant (mc$^2$7852) was inoculated in 7H9 medium or in 7H9 medium supplemented with hemin (100 μM) or MbJ (200 ng/mL). For 7H9 medium, growth curves are in duplicate. Data points represent the mean ± SEM; growth curves for 7H9 + hemin and 7H9 + MbJ were performed in singlicate. (*D*) The acquisition of $^{55}$Fe-loaded cMb was assessed for WT (mc$^2$6230) and Δ*esx-3* (mc$^2$7818) at 37 °C and 4 °C.

mutant was highly impaired for growth in 7H9 medium, even with supplementation (Fig. 2*C*). Therefore, although *esx-3* mutants accumulate Mb, this excess siderophore does not account for the growth defect.

To verify that *esx-3* plays a role in siderophore uptake, we examined the accumulation of $^{55}$Fe-loaded cMb by WT and Δ*esx-3*. At 37 °C, Δ*esx-3* accumulated <50% of the radiolabel acquired by the parental strain (Fig. 2*D*), although the strains exhibited similar levels of nonspecific adsorption at 4 °C. Although uptake of $^{55}$Fe-cMb was substantially less for Δ*esx-3* than for WT, it was not completely absent, supporting the idea that a lower-affinity Mb uptake system functions in the absence of *esx-3*. Taken together, these results substantiate a role for *esx-3* in siderophore-mediated iron acquisition.

**Virulence Role of *pe5–ppe4* and *mbtB* Depends on Host Genotype.** To assess the virulence of numerous mutant strains rapidly, we initially infected BALB/c SCID mice by the i.v. route. A dose of $10^4$ cfu of H37Rv was lethal by ∼40 d postinfection, whereas mice survived ∼$10^7$ cfu of Δ*esx-3* (Fig. 3*A*). Despite their strikingly similar in vitro iron-related growth defects, mutants harboring individual deletions within the *esx-3* region were less severely attenuated. After infection of SCID mice with ∼$2 \times 10^6$ cfu, the median survival time (MST) was 22 d for mice infected with the WT strain, 27 d for mice infected with Δ*mbtB* and Δ*pe5–ppe4*, and 65 d for mice infected with Δ*esxH*; this substantial attenuation of Δ*esxH* was largely reversed by genetic complementation (Fig. 3*B*). Most dramatically, the Δ*esx-3*–infected mice survived for 12 mo, whereas complementation of Δ*esx-3* resulted in slight hypervirulence (MST 19 d). The relatively modest attenuation of Δ*pe5–ppe4* and Δ*mbtB* was surprising, given their profound phenotypes in vitro. To address whether hemin supplementation in the growth medium used before i.v. infection provided iron stores that the bacteria could use in vivo, we examined the virulence of the strains following growth in different amounts of hemin. For Δ*mbtB*, the kinetics of mortality were nearly identical if bacteria were pregrown in 5 or 100 μM hemin (MST 30 d; Fig. 3*C*). Similarly, when the Δ*pe5–ppe4* mutant was cultured in the absence of hemin, it was only mildly attenuated (Fig. 3*C*), similar to when it was pregrown in 100 μM hemin (Fig. 3*B*). These results show that, despite their profound growth defects in vitro, the Δ*pe5–ppe4* and Δ*mbtB* mutants are only mildly attenuated in vivo.

The SCID mice used here were in the BALB/c background, which is defective in natural resistance-associated macrophage protein 1 (Nramp1) (29), a metal transporter localized to the endosomal compartment of macrophages that may restrict phagosomal iron (30). In inbred mouse strains, *nramp1* is found in two allelic forms, *nramp1*$^R$ (resistant) and *nramp1*$^S$ (susceptible); the susceptible allele results in degradation of the protein and susceptibility to a variety of intracellular pathogens (31). Nramp1 is functional in CBA mice (29), which we challenged by i.v. infection with ∼$2 \times 10^6$ cfu of H37Rv, Δ*mbtB* grown in high or low hemin, or Δ*pe5–ppe4*. Strikingly, in contrast to observations in the *nramp1*$^S$ mice, Δ*pe5–ppe4* and Δ*mbtB* were highly attenuated in *nramp1*$^R$ CBA mice (Fig. 3*D*). These data demonstrate a host-dependent requirement for ESX-3 substrates.

**Δ*esx-3* and Δ*esxH* Are Attenuated for Growth in Human Macrophages, but Intracellular Growth of Δ*pe5–ppe4* Depends on Macrophage Polarization.** Differences in iron handling have been described for classically (M1) as opposed to alternatively (M2) activated macrophages (32, 33). Similar observations have been made for human macrophages differentiated with macrophage colony-stimulating factor (M-CSF) versus GM-CSF (34), where GM-CSF may promote a more iron-restrictive state. We therefore examined the growth of Δ*esx-3*, Δ*esxH*, and Δ*pe5–ppe4* in human macrophages differentiated with M-CSF or GM-CSF (Fig. S4). The Δ*esx-3* and Δ*esxH* mutants were highly attenuated for growth in human macrophages, regardless of the cytokine used for differentiation. However, Δ*pe5–ppe4* showed a modestly improved growth capacity

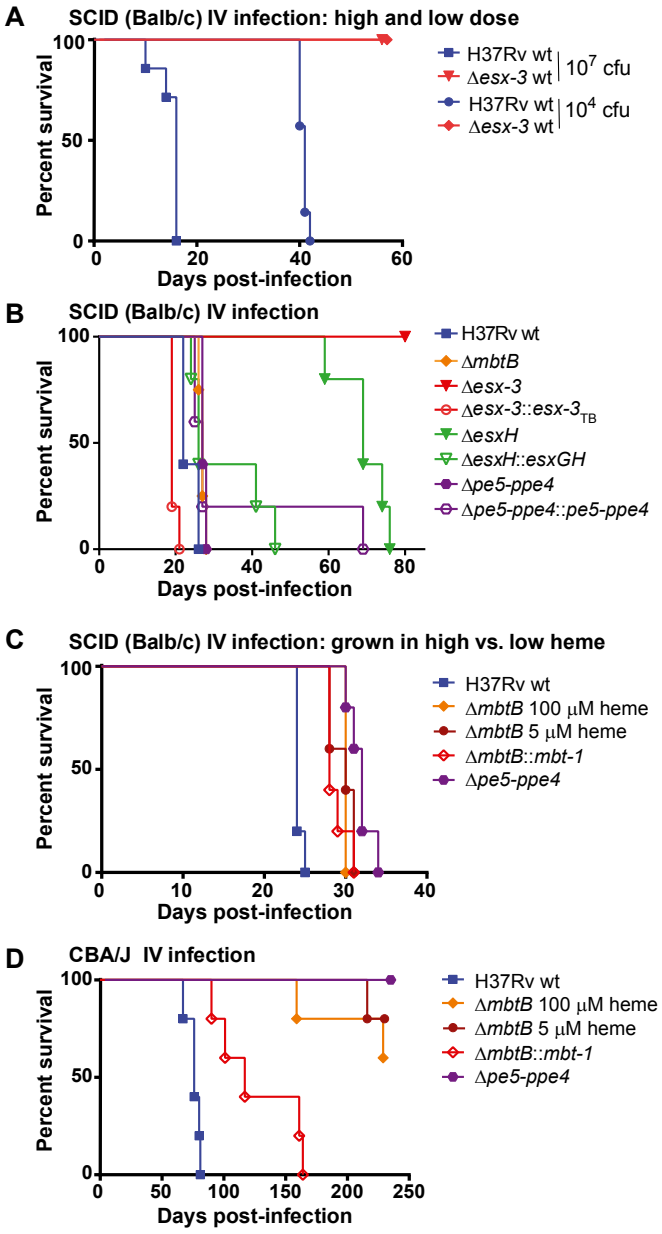


**Fig. 3.** Deletion of the entire *esx-3* locus results in dramatic attenuation in vivo, but *pe5–ppe4* and *mbtB* are required for virulence in a mouse strain-dependent manner. (*A* and *B*) Survival of SCID mice infected by the i.v. route with H37Rv or Δ*esx-3* (mc$^2$7788) at ∼$10^4$ or ∼$10^7$ cfu (*A*) or with H37Rv WT, Δ*mbtB* (mc$^2$7850), Δ*esx-3* (mc$^2$7844), Δ*esx-3*::*esx-3*$_{TB}$ (mc$^2$7856), Δ*esxH* (mc$^2$7846), Δ*esxH*::*esxGH* (mc$^2$7867), Δ*pe5–ppe4* (mc$^2$7848), or Δ*pe5–ppe4*::*pe5–ppe4* (mc$^2$7868) at a dose of ∼$2 \times 10^6$ cfu (*B*). $n = 7$ or 8 mice per group in *A* and 4 or 5 mice per group in *B*. Before the infections shown in *A* and *B*, bacteria were cultured in 7H9 medium with 100 μM hemin. (*C*) Survival of SCID mice infected by the i.v. route with H37Rv, Δ*mbtB* (mc$^2$7850) pregrown in 100 μM hemin or 5 μM hemin, the Δ*mbtB*::*mbt-1* complemented strain (mc$^2$7874), or Δ*pe5–ppe4* (mc$^2$7848). Except for the indicated Δ*mbtB* strains, the strains were grown without hemin. $n = 5$ mice per group. (*D*) Survival of CBA mice infected by the i.v. route with the strains in *C*. $n = 5$ mice per group. Survival differences were assessed using the log-rank (Mantel–Cox) test. In *B*, all groups were significantly different ($P < 0.05$) from WT except Δ*esxH*::*esxGH* and Δ*pe5–ppe4*::*pe5–ppe4*. In *C* and *D*, all groups differed significantly ($P < 0.05$) from WT. In *C*, survival of mice infected with Δ*mbtB* grown in 100 μM hemin did not differ significantly from that of mice infected with Δ*mbtB* grown in 5 μM hemin or with the Δ*mbtB*::*mbt-1* complemented strain. In *D*, survival of mice infected with Δ*mbtB*::*mbt-1* differed significantly from that of mice infected with the Δ*mbtB* strains.

(~2.4-fold) in the M-CSF–differentiated macrophages, indicating that the requirement for *pe5–ppe4* may differ depending upon macrophage polarization, possibly resulting in differences in iron handling of M-CSF– versus GM-CSF–differentiated cells. In contrast, Δ*esx-3* and Δ*esxH* were essential for intracellular growth irrespective of macrophage polarization.

**The in Vitro Iron Phenotype Does Not Correlate with Virulence in SCID or Recombination-Activating Gene Knockout Mice.** To explore further the relationship between the iron phenotype and virulence, we compared Δ*esx-3* complemented with the Mtb *esx-3* region and a strain complemented with the Msmeg *esx-3* region. Although the Msmeg *esx-3* region complemented the in vitro iron-related growth defects of Δ*esx-3* (Fig. 4*A*), only the Mtb *esx-3* region restored growth in vivo. Infection with Δ*esx-3::esx-3*$_{SMEG}$ did not result in any mortality (Fig. 4*B*), even after 12 mo of infection. Therefore, despite the substantial homology between the Msmeg and Mtb *esx-3* regions (14), Msmeg *esx-3* lacks functions necessary for virulence. Additional evidence that virulence is separable from the iron requirement comes from analysis of a Δ*esxG* mutant expressing an aberrant EsxG protein product that has 12 additional N-terminal amino acids (referred to as "*esxGH*$^{**12aa}$; pJP148") (Table S2). Remarkably, the in vitro phenotype of the hygromycin-marked Δ*esxG* strain (mc$^2$7789) was rescued by the EsxG$^{**12aa}$ variant even though EsxG–EsxH secretion was nearly undetectable on Western blotting (Fig. 4 *C* and *D*). This finding is consistent with reports in Msmeg, in which <1% of EsxG–EsxH secretion reversed the iron-related growth defects (12). Despite correcting the iron-related growth defect, the strain complemented with EsxG fused to 12 N-terminal amino acids (Δ*esxG*::*esxGH*$^{**12aa}$) behaved almost identically to Δ*esxG* in recombination-activating gene knockout (*RAG1*$^{-/-}$) mice (Fig. 4*E*). Interestingly, although able to restore growth of Δ*esxG* on solid medium, the same plasmid (pJP148) was unable to rescue growth of Δ*esx-3* (Fig. 4*F*), implying that EsxG–EsxH secretion in Mtb is dependent on the presence of *esx-3*, consistent with findings in Msmeg (13).

***esx-3* and *esxH* Are Essential for Virulence in Aerosol Infections, but *pe5–ppe4* and *mbtB* Are Dispensable.** We next sought to determine whether the differences in virulence between strains also would be observed in a model that more closely mimics the natural infection. We infected C57BL/6 (*nramp1*$^S$) mice by aerosol with WT, Δ*esx-3*, and Δ*esx-3::esx-3*$_{TB}$ strains. In contrast to WT, the Δ*esx-3* mutant could not be recovered from the lungs, and it failed to disseminate to the spleen; Δ*esx-3::esx-3*$_{TB}$ was mildly hypervirulent (Fig. 5 *A* and *B*). Similarly, Δ*esxH* did not proliferate in vivo, failed to disseminate, and was complemented by expression of *esxG–esxH* (pYUB1944) (Fig. 5 *C* and *D*). The marked attenuation of Δ*esx-3* and Δ*esxH* was in striking contrast to the Δ*pe5–ppe4* and Δ*mbtB* mutants, for which bacterial numbers were similar to WT (Fig. 5 *C* and *D*). Overall, these findings support the idea that defects in iron acquisition do not underlie the dramatic in vivo attenuation of Δ*esx-3*. Rather *esx-3* must play an additional role in virulence that is dependent upon EsxH and independent of PE5–PPE4.

**Identification of Rv1386 (PE15)/Rv1387 (PPE20) as ESX-3–Secreted Substrates.** To elucidate further the role(s) played by *esx-3* in iron acquisition and virulence, we sought to define the secreted effectors. CF from triplicate samples of WT, Δ*esx-3*, Δ*esxG*, Δ*esxH*, Δ*esx-3::esx-3*$_{TB}$, Δ*esx-3::esx-3*$_{SMEG}$, and Δ*mbtB* cultured in chelated Sauton's medium was analyzed by MS using the MaxQuant software suite with the Andromeda search engine for peptide identification (*SI Materials and Methods* and Fig. S5). Label-free quantitation (LFQ) algorithms were used to determine relative protein amounts (*SI Materials and Methods*) (35). A panel of ribosomal and chaperonin proteins (Dataset S2) was used to verify similar amounts of lysis in the samples (Fig. S5*B*). Correcting for multiple testing by controlling for a false discovery rate (FDR) at 5% using the Benjamini–Hochberg method (36), we detected 854 proteins in total (Dataset S2), of which 72 were differentially secreted in the WT strain compared with Δ*esx-3* (Fig. 6*A*, and *SI Materials and Methods*, and Fig. S6*A*). Esx proteins encoded outside the *esx-3* locus that could be unambiguously

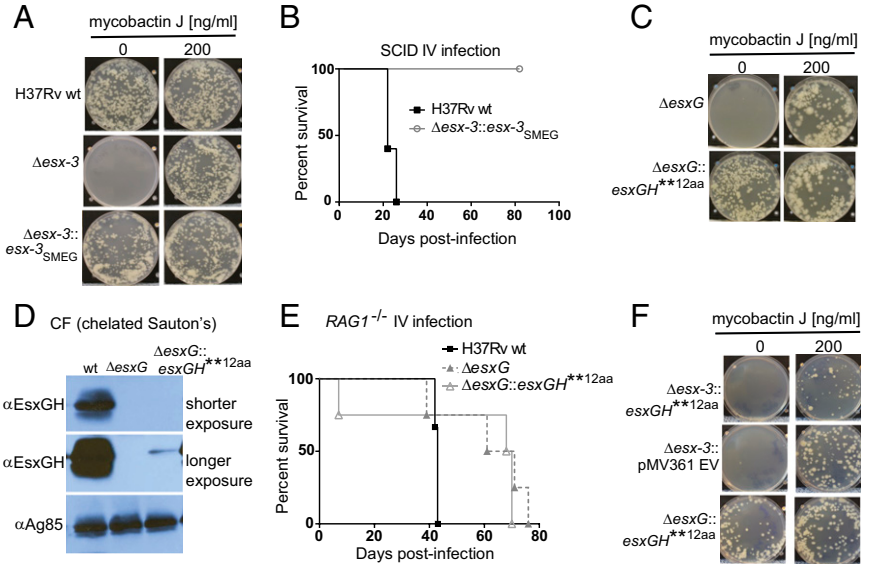


**Fig. 4.** *esx-3* from Msmeg and the EsxG variant restore in vitro growth but not virulence to *esx-3* region mutants. (*A*) H37Rv WT, Δ*esx-3* (mc$^2$7844), and Δ*esx-3*::*esx-3*$_{SMEG}$ (mc$^2$7857) were plated on 7H10 medium with or without MbJ (200 ng/mL). (*B*) Survival of BALB/c SCID mice infected i.v. with H37Rv or Δ*esx-3*::*esx-3*$_{SMEG}$ (mc$^2$7857). $n = 5$ mice per group. (*C*) Δ*esxG* (mc$^2$7789) and Δ*esxG* transformed with pJP148 (mc$^2$7830) were plated on 7H10 medium and on 7H10 medium with 200 ng/mL MbJ. (*D*) CF from strains grown in chelated Sauton's medium was analyzed by Western blotting using an antibody raised against the EsxG–EsxH complex and was compared with H37Rv. Ag85B served as a loading control. (*E*) Survival analysis of C57BL/6 *RAG1*$^{-/-}$ mice infected by the i.v. route with ~$5 \times 10^4$ cfu of H37Rv, Δ*esxG* (mc$^2$7789), or Δ*esxG* harboring pJP148 (mc$^2$7830). $n = 3$ mice for H37Rv WT and 4 mice for the other strains. (*F*) Δ*esx-3* transformed with pMV361 empty vector (EV) (mc$^2$7831) and Δ*esx-3* or Δ*esxG* transformed with pJP148 (mc$^2$7829 and mc$^2$7830, respectively) were plated on 7H10 medium and on 7H10 medium with 200 ng/mL MbJ.

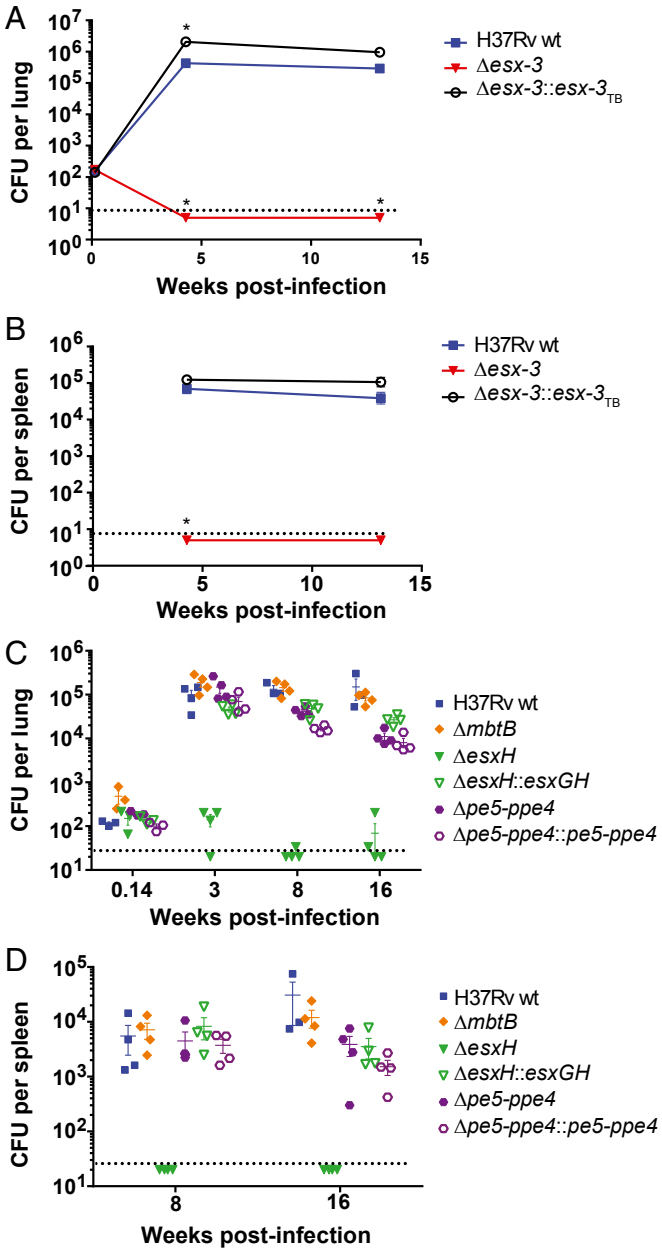


**Fig. 5.** Δ*esx-3* and Δ*esxH* are severely attenuated in aerosol infection of C57BL/6 mice, but Δ*pe5–ppe4* and Δ*mbtB* remain virulent. (*A* and *B*) Bacterial burdens in lungs (*A*) and spleens (*B*) were determined at the indicated time points after aerosol infection with H37Rv, Δ*esx-3* ($mc^2$7788), or Δ*esx-3*::*esx-3*$_{TB}$ ($mc^2$7827). $n = 4$ or 5 mice per group, except $n = 3$ for H37Rv-infected spleens at 4 wk. Data points indicate mean ± SEM. Data points that are significantly different ($P < 0.05$) from H37Rv WT using an unpaired Student's *t* test are indicated by an asterisk. (*C* and *D*) Following aerosol infection with the indicated strains, bacterial burdens were determined at 24 h and at 3, 8, and 16 wk postinfection in lungs (*C*) and at 8 and 16 wk postinfection in spleens (*D*). Strains were H37Rv, Δ*mbtB* ($mc^2$7850), Δ*esxH* ($mc^2$7846), Δ*esxH*::*esxGH* ($mc^2$7867), Δ*pe5–ppe4* ($mc^2$7848), and Δ*pe5–ppe4*::*pe5–ppe4* ($mc^2$7868); all strains were cultured in 7H9 medium supplemented with 100 μM hemin before use in aerosol infections. Individual data points are shown; lines indicate mean ± SEM. $n = 3$ or 4 mice per group. Dotted lines indicate approximate limits of detection.

identified, including EsxA, EsxB, EsxL, EsxN, and EsxO, were present in similar amounts in both samples, demonstrating that the *esx-3* deletion does not globally impair Esx protein secretion (Fig. 6*A*). As expected from analogy to EsxA and EsxB, EsxG and EsxH exhibited codependent secretion; EsxH was present at greatly diminished levels in the CF of the Δ*esxG* mutant compared with WT, and similarly EsxG was present at greatly reduced levels in the CF of Δ*esxH* (Fig. 6 *B* and *C* and Figs. S5*C* and S6 *B* and *C*). Genetic complementation resulted in partial restoration of both EsxG and EsxH secretion in both mutants (Fig. S6 *B* and *C*).

To identify ESX-3 substrates, we focused on eight proteins that were present in all three WT samples and were diminished in Δ*esx-3* (Fig. 6 *A*, *E*, and *G* and Fig. S6). Of these, secretion of Rv1009/RpfB was not restored by complementation (Dataset S2), suggesting that it may not be a substrate for secretion. Of the remaining proteins, five (Rv0282, Rv0283, Rv0285/PE5, EsxG, and EsxH) were encoded within the region deleted in the mutant strain. We detected trace levels of these five proteins in the Δ*esx-3* samples (below 3% of WT levels), consistent with a typical level of carryover. To verify this result, we reran one sample from each strain on an extensively washed column; as expected, these proteins were not detected (Fig. S5*C*). Rv1387/PPE20 and Rv2477c were the only other proteins that satisfied our criteria for being potential substrates. However, Rv2477c also was undetectable in two of three Δ*mbtB* samples (Dataset S2), suggesting that its absence might reflect an adaptation to iron deprivation as opposed to its being a direct ESX-3 substrate. Thus, only Rv1387/PPE20 fulfilled criteria as a potential ESX-3 substrate. Although it did not meet our strict criteria for significance, Rv1386 (PE15) also was diminished in the *esx-3* mutant (*P* value 0.007, which corresponds to an FDR of 13%) (Fig. 6*A*) and was undetectable when the Δ*esx-3* sample was reanalyzed after carryover removal (Fig. S5*C*). CF samples prepared from Δ*esxG* and Δ*esxH* also had greatly reduced or undetectable PE15 and PPE20 (Fig. 6 *B* and *C* and Figs. S5*C* and S6 *B* and *C*), demonstrating that secretion of these proteins is dependent on EsxG and EsxH. Combined, these data strongly suggest that PE15 and PPE20 are ESX-3 substrates.

**Secretion of PE5–PPE4 Is Required for Iron Acquisition, Whereas Secretion of EsxG and EsxH Is Important for Virulence.** We next examined whether secretion of EsxG–EsxH and PE5–PPE4 are codependent. Although still detectable, secretion of PE5 was substantially reduced in Δ*esxG* and Δ*esxH* (Fig. 6 *B* and *C* and Figs. S5*C* and S6*B*). This diminution reached significance for Δ*esxG* but not for Δ*esxH*, using our strict criteria [*P* values for PE5 of 0.0003 (FDR = 6%) in WT vs. ΔesxG and 0.001 (FDR 26%) in WT vs. ΔesxH]. We did not detect PPE4 in the CF of any sample, and this protein likely remains membrane localized because it contains several hydrophobic, potentially membrane-spanning domains, analogous to the situation in ESX-1, where PE35 is found in the CF and PPE68 remains membrane associated (37, 38). In contrast, the Δ*pe5–ppe4* mutant secreted nearly WT levels of EsxG and EsxH (Figs. S5*C* and S6*D*), a finding confirmed on Western blotting using a polyclonal antibody recognizing the EsxG–EsxH complex (Fig. 6*I*). Thus, the Δ*pe5–ppe4* mutant exhibits a severe iron phenotype but secretes EsxG and EsxH normally and is not attenuated in vivo in *nramp1*$^S$ hosts. This observation shows that the iron-acquisition function of ESX-3 is not simply related to the secretion of EsxG–EsxH. Taken together with the phenotypic studies, the data suggest that PE5–PPE4 is important for the iron-acquisition function of ESX-3, whereas virulence correlates with secretion of EsxG, EsxH, PE15, and PPE20 (Fig. 6*J*).

## Discussion

Mtb encodes five evolutionarily related T7SS, ESX-1–ESX-5 (7, 39–41). These systems are believed to influence the outcome of infection by directing the secretion of specific effector proteins. However, apart from the intensively investigated ESX-1, there are limited data characterizing the secretomes of individual ESX systems or correlating these findings with in vivo data to define the contributions of individual effectors to pathogenesis. This undertaking is complex, because ESX systems have been shown to secrete a variety of substrates lacking classical N-terminal

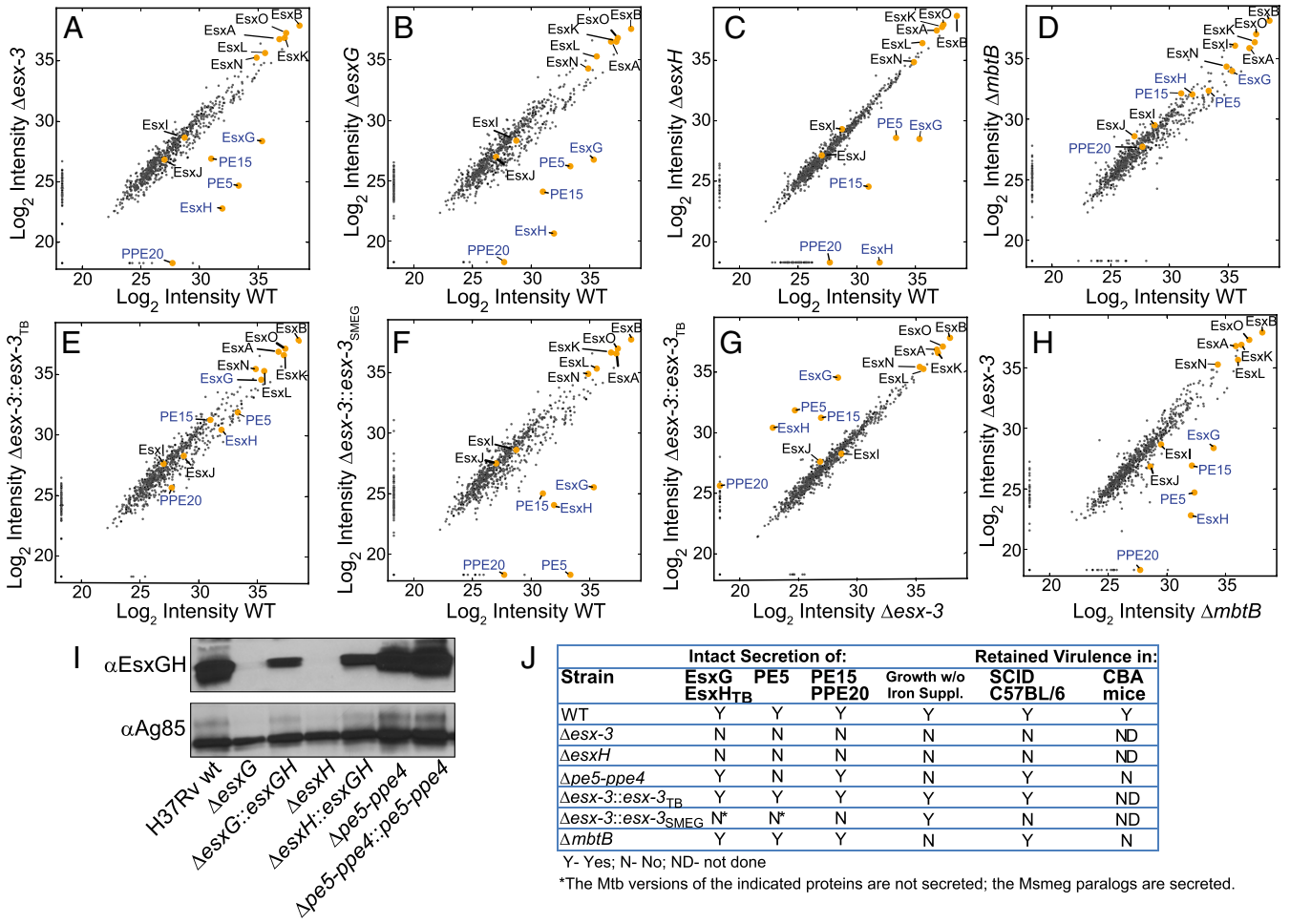


J

| Strain | Intact Secretion of: EsxG EsxH$_{TB}$ | PE5 | PE15 PPE20 | Growth w/o Iron Suppl. | Retained Virulence in: SCID C57BL/6 | CBA mice |
|---|---|---|---|---|---|---|
| WT | Y | Y | Y | Y | Y | Y |
| Δ*esx-3* | N | N | N | N | N | ND |
| Δ*esxH* | N | N | N | N | N | ND |
| Δ*pe5-ppe4* | Y | N | Y | N | Y | N |
| Δ*esx-3*::*esx-3*$_{TB}$ | Y | Y | Y | Y | Y | ND |
| Δ*esx-3*::*esx-3*$_{SMEG}$ | N* | N* | N | Y | N | ND |
| Δ*mbtB* | Y | Y | Y | N | Y | N |

Y- Yes; N- No; ND- not done

*The Mtb versions of the indicated proteins are not secreted; the Msmeg paralogs are secreted.

**Fig. 6.** Proteomics MS analysis of CF reveals codependent secretion of PE5 with EsxG–EsxH and identifies PE15/PPE20 as ESX-3 substrates. (*A*–*H*) Scatterplots show $\log_2$-transformed LFQ intensity values of proteins identified in the CF with the following strain comparisons: H37Rv vs. Δ*esx*-3 (mc$^2$7844) (*A*); H37Rv vs. Δ*esxG* (mc$^2$7845) (*B*); H37Rv vs. Δ*esxH* (mc$^2$7846) (*C*); H37Rv vs. Δ*mbtB* (mc$^2$7850) (*D*); H37Rv vs. Δ*esx-3*::*esx-3*$_{TB}$ (mc$^2$7827) (*E*); H37Rv vs. Δ*esx-3*::*esx-3*$_{SMEG}$ (mc$^2$7828) (*F*); Δ*esx-3* vs. Δ*esx-3*::*esx-3*$_{TB}$ (*G*); and Δ*mbtB* vs. Δ*esx-3* (*H*). Values for proteins of interest (Esx proteins and select PE–PPE proteins) are in yellow and are labeled; proteins implicated as ESX-3 substrates are indicated by blue text. Trace amounts of PE5, EsxG, and EsxH were detected in the Δ*esx-3* samples because of carryover from other samples; when the columns were washed extensively between runs, PE5, EsxG, and EsxH were absent from Δ*esx-3*, as anticipated (Fig. S5*C*). See Fig. S6 for lists of proteins that are present at significantly different levels for the various comparisons and Dataset S2 for lists of all proteins detected in the secretome analysis. (*I*) Western blot analysis of CF from strains grown in chelated Sauton's medium using the EsxG–EsxH antibody. Ag85B served as a loading control. (*J*) Summary of secretome findings, in vitro growth requirements, and in vivo growth characteristics for the various strains.

signal sequences, including Esx family members, members of the diverse PE and PPE protein families, and, in some cases, additional substrates (such as Esp proteins secreted via ESX-1) (41). The studies of ESX-3 described here demonstrate how a single ESX system can secrete multiple effectors to modulate varied host defenses to influence pathogenesis.

Previous findings have suggested that ESX-3 functions in the acquisition of iron (11, 13); in the context of host infection, this iron-uptake capacity is of critical importance to nearly all bacterial pathogens (42, 43). Here, using a panel of Mtb deletion mutants, we demonstrate that not only the entire *esx-3* locus but specifically the secreted substrates EsxG–EsxH and PE5–PPE4 are required for iron acquisition. We further demonstrate that the contribution of iron acquisition to Mtb virulence in human macrophages and mouse models depends on the host phenotype. Remarkably, analysis of the *esx-3* region mutants showed that ESX-3 plays a critical role in virulence, which correlates with the secretion of effectors distinct from those required for iron acquisition (Fig. 6*J*). Although all mutants required iron supplementation to grow on solid medium, we found striking differences in their impact on virulence in mice. The Δ*pe5–ppe4* and Δ*mbtB* strains, which retained the ability to secrete EsxG–EsxH and PE15–PPE20, were virulent in i.v. infections of SCID mice and aerosol infections of C57BL/6 mice; this virulence may reflect the ability of Mtb to exploit in vivo sources of iron such as heme (20, 21). Still, this result was surprising, given the reported phenotype of other mutants defective in Mb synthesis or trafficking. Some of the data are not directly comparable to ours, because the other studies used bacillus Calmette–Guérin rather than Mtb or guinea pigs rather than a murine model (27, 44). However, both *mbtK*, which transfers fatty acids to the Mb peptide core, and *mmpS4*/*S5*, which are required for siderophore export, are essential for virulence in mice (45, 46). Notably, however, both of these mutants also have additional phenotypes (altered lipid profiles and toxic accumulation of siderophores, respectively) that could contribute to their in vivo attenuation (28, 45). In contrast to Δ*pe5–ppe4* and Δ*mbtB*, the Δ*esxH* mutant behaved similarly to the strain bearing a deletion of the entire *esx-3* region in aerosol infections of C57BL/6 mice. Both Δ*esxH* and Δ*esx-3* were substantially attenuated, failing to proliferate in the lungs and to disseminate to the spleen. This finding suggests that the virulence defect of Δ*esx-3* is not caused solely by defective iron acquisition and further suggests that the attenuation is primarily attributable to absence of EsxH, either directly

or through the loss of other substrates that rely on EsxH for secretion.

We considered the possibility that the requirement for iron-acquisition systems in Mtb might depend on the capacity of the host to restrict iron by comparing infection in mouse lines that differ in the *nramp1* gene (29, 47). Nramp1 is thought to export divalent metals out of the phagosome, and that export is postulated to starve bacteria of essential metals and/or to heighten oxidative stress (30). Remarkably, both the Δ*mbtB* and Δ*pe5–ppe4* mutants were highly attenuated in *nramp1*$^{R}$ CBA mice, in contrast to their relatively preserved virulence in the *nramp1*$^{S}$ mice (C57BL/6 and BALB/c). Interestingly, an extensive body of literature suggests that the *nramp1*$^{R}$ locus does not confer resistance to infection with fully virulent Mtb in mice (48, 49), although in humans polymorphisms in *NRAMP1* (termed "*SLC11A1*") are associated with the development of pulmonary tuberculosis in West African and Asian populations (50, 51). The *pe5–ppe4* and *mbtB* mutants, with defects related to iron utilization, may reveal a role of Nramp1 in host defense against Mtb and point to siderophore-mediated iron uptake as an immune evasion mechanism. Of course, additional differences between the inbred strains also could underlie the distinct phenotypes (52, 53), and further studies using congenic strains will clarify the contribution of Nramp1. Our macrophage data also indicate that the importance of *pe5–ppe4* for intracellular growth of Mtb may depend on macrophage gene expression and polarization. Overall, our studies reveal a relationship between host genotype and bacterial iron handling in determining the outcome of infection with Mtb.

Our proteomic analysis points to a limited set of ESX-3–secreted substrates: EsxG, EsxH, the PE–PPE pair encoded within the locus (PE5–PPE4), an evolutionarily related pair of proteins encoded outside the locus (PE15–PPE20), and perhaps a few others such as Rv2477c. However, Rv2477c lacks the characteristic YxxxD/E T7SS motif and also is reduced in CF from Δ*mbtB*, making its assignment as a direct ESX-3 substrate less likely. The limited number of substrates assigned to the Mtb ESX-3 secretion system differs somewhat from ESX-1, which secretes a number of Esp substrates, and from ESX-5, which appears to secrete multiple PE–PPE family members (41). However, additional ESX-3 effectors may remain membrane associated and undetectable in CF or may be secreted under culture conditions different from those tested here. Nonetheless, several features of ESX-1 and ESX-5 also appear to be shared by ESX-3. EsxG and EsxH, which form a heterodimer (15, 54), exhibited codependent secretion, as did EsxA and EsxB (55, 56). In addition, elimination of EsxG or EsxH impaired the secretion of PE5 and PE15–PPE20. This suggests that EsxG may behave like its counterpart EsxB, which recently has been shown to promote the ATPase activity of the secretion apparatus (57).

Our data also clearly support the observation that specific PE–PPE pairs are targeted to specific ESX systems (58, 59). To our knowledge, PE15–PPE20 is the first PE–PPE pair encoded outside an *esx* locus for which the data support secretion by an ESX system other than ESX-5. It is not surprising that ESX-3 secretes this pair, because there is a strong connection between PE5 and PE15: They are evolutionarily closely related (60) and are highly conserved in members of the Mtb complex, share 67% identity, and are suggested to play role(s) in intracellular survival in macrophages (61). Moreover, their relationship is underscored by transcriptional data, because both *pe5–ppe4* and *pe15–ppe20* appear to belong to the ZuR regulon (62, 63) and are down-regulated by nutrient starvation (64). Interestingly, however, two lines of evidence suggest that PE15 and PPE20 are not responsible for the iron-acquisition function of ESX-3. First, complementation of Δ*esx-3* with *esx-3*$_{SMEG}$ corrected the in vitro growth defect (Fig. 4*A*) but failed to restore secretion of PE15/PPE20 (Fig. 6*F*). Second, Δ*pe5–ppe4* exhibited iron-related growth defects very similar to Δ*esx-3* but secreted PE15/PPE20 in excess of WT (Fig. S5*C*). Our finding that the Δ*pe5–ppe4* mutant has preserved secretion of EsxG/EsxH is also consistent with findings from genetic analysis of the ESX-1 locus, where deletion of *ppe68* resulted in a modest increase in EsxA secretion (55, 65). However, the data are more complex for ESX-5, in which deletion of the *ppe25–pe19* gene cluster in H37Rv led to loss of EsxN and PPE41 secretion (66), although differing results were obtained for a *ppe27* mutant in the CDC1551 background (67).

In summary, our findings implicate the PE5–PPE4 proteins as the critical ESX-3 effectors involved in iron acquisition. EsxG–EsxH may be required for iron utilization simply by virtue of promoting PE5–PPE4 secretion, or both complexes may act in concert to assimilate Mb-bound iron (see the model in Fig. 7). Our data also indicate that ESX-3 regulates Mtb growth and virulence in vivo in a manner independent of the iron-acquisition functions that are so critical in vitro. This regulation may be related to recent observations that the ESX-3 region can modulate host immune responses; removal of the Msmeg *esx-3* region attenuated the organism as the result of clearance by an MyD88-dependent innate immune response (14). Further, EsxH has been demonstrated to interact with and inhibit the mammalian cell ESCRT machinery that plays critical roles in membrane trafficking (19). Additional studies will be required to elucidate the in vivo functions of EsxG–EsxH and to clarify how ESX-3 facilitates iron acquisition and under what circumstances different ESX-3 effector proteins are required for virulence. Finally, this work reinforces the significance of T7SS for mycobacterial–host interactions and highlights the need for continued investigation into their role in pathogenesis.

## Materials and Methods

**Bacterial Strains.** Mtb H37Rv and mc$^{2}$6230 (H37Rv Δ*RD1* Δ*panCD*) were used to generate mutants as listed in Table S1. Mutants were constructed using specialized transduction (68, 69). The antibiotic cassette was removed from selected strains using phage-delivered γδ-resolvase, with *sacB* counterselection facilitating the isolation of unmarked strains (69). The L5 phage integration system was used for complementation. Details of strain and plasmid construction are provided in *SI Materials and Methods*.

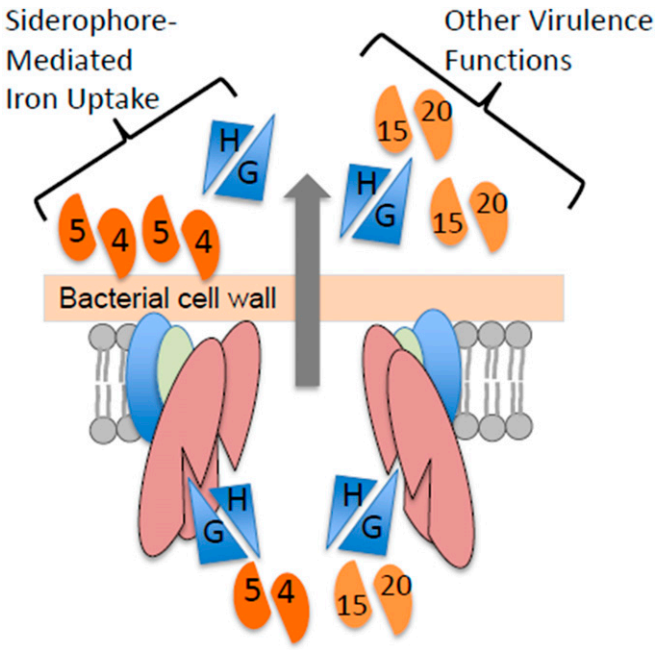


**Fig. 7.** The schematic illustrates ESX-3 substrates and their distinct functional roles. EsxG and EsxH are cosecreted and facilitate secretion of PE5–PPE4 (the latter remaining membrane-localized). PE5–PPE4, perhaps in concert with EsxG–EsxH, plays a role in siderophore-mediated iron uptake. EsxG and EsxH also facilitate secretion of PE15–PPE20, and, separately or together, these proteins play additional, iron-independent roles in virulence.

**Liquid Growth Conditions.** Mycobacterial strains were cultured at 37 °C in Middlebrook 7H9 medium (Difco) with 10% (vol/vol) oleic acid-albumin-dextrose-catalase (OADC) enrichment (BBL; Becton Dickinson), 0.2% glycerol (Fisher), and 0.05% Tween 80 or 0.05% tyloxapol (referred to as "7H9"), with additional supplements as indicated. Strains bearing antibiotic cassettes were cultured with 50–75 μg/mL hygromycin or 25 μg/mL kanamycin as appropriate. Chelated Sauton's medium consisted of 0.5 g $KH_2PO_4$, 4 g L-asparagine·$H_2O$, 2 g citric acid, 60 g glycerol/L, adjusted to pH ∼7.0, and treated overnight with chelex-100 (10 g/L) (Bio-Rad) to remove trace iron contaminants. After filtration, 0.5 g/L of $MgSO_4 \cdot 7H_2O$ was added.

**Solid Medium Growth Experiments.** Bacterial cultures were washed in PBS containing 0.05% Tween 80 or 0.05% tyloxapol (PBS-T), were resuspended in PBS-T, and were adjusted to equivalent $OD_{600}$ values. Serial dilutions were plated onto 7H10 base medium containing 10% OADC and 0.5% glycerol with additional additives as indicated. Supplements included bovine hemin (Sigma), 0.05% Tween 80, FAC (Sigma), zinc sulfate (Sigma or Fisher), and MbJ (Allied Monitor). Plates were incubated for ∼3–6 wk at 37 °C.

**Liquid Growth Curves.** Bacteria were cultured in 7H9 medium with ∼5 μM residual hemin from the frozen stock. In some experiments 10 μM hemin was added to promote growth of Δ*mbtB*; 100 μM hemin was added for the Δ*esx-3* Δ*mbt-1* double mutant. Bacteria were pelleted by centrifugation, washed in PBS-T, and inoculated into growth medium at a starting $OD_{600}$ of ∼0.02. Medium was unsupplemented 7H9 or included 100 μM 2,2′-dipyridyl (Sigma), 100 μM hemin, or 200 ng/mL MbJ. MbJ was prepared as described (27) by solubilizing 100 μg in a solution containing 250 μg tyloxapol in 1.25 mL ethanol (20% wt/vol). The ethanol was evaporated under vacuum, and the tyloxapol and MbJ were resuspended in 7H9 medium and added to 500 mL 7H9.

**Siderophore Uptake and Synthesis.** Uptake of cMb was quantified as described previously (46), using Msmeg cMb, which was deferrated and then labeled with $^{55}Fe$ (see *SI Materials and Methods* for details). Analysis of radiolabeled siderophores from Mtb grown in iron-deficient medium and extraction of unlabeled siderophores from iron-replete cultures was performed essentially as described previously (46); additional details are provided in *SI Materials and Methods*. For MS analysis of siderophores, strains were cultured in 7H9 medium with 24 μg/mL D-pantothenate. Cell pellets were washed with PBS and were extracted with $CHCl_3$/MeOH (2:1). Two and a half milliliters of sterile filtered supernatants were acidified with 15 μL 3M HCl and extracted with 3.5 mL ethyl acetate (70). The organic phases of pellet and supernatant extractions were dried, resuspended in isopropanol/acetonitrile/water (2:1:1; vol/vol/vol), and subjected to ultra high-performance liquid chromatography (UPLC)-MS analysis as described in *SI Materials and Methods* and ref. 71.

**Intracellular Bacterial Growth Assays.** Human macrophages were prepared as described (72) following the method of Vogt and Nathan (73) and differentiation with either 2 ng/mL recombinant human GM-CSF or 10 ng/mL recombinant human M-CSF (R&D Systems), as detailed in *SI Materials and Methods*. Following infection at a multiplicity of infection (MOI) of 0.02, mycobacterial growth was enumerated at 14 d postinfection by plating on 7H10 plates containing 200 ng/mL MbJ (Allied Monitor). Colonies were counted after ∼2–3 wk of incubation.

**CF Preparation.** CFs were prepared as described (19). Following growth to log phase in 7H9 medium (with 10 μM hemin for the Δ*mbtB* strain), Mtb were subcultured for 2 d in chelated Sauton's medium, pelleted by centrifugation, and the supernatants were filtered through 0.22-μM filters followed by precipitation with 12% trichloroacetic acid (TCA) (also see *SI Materials and Methods*).

**Proteomics MS.** Protein pellets were reconstituted in 2-M urea buffer, pH 7.8, before reduction, alkylation, and digestion with trypsin. After desalting the peptide mixtures were gradient eluted directly into a Q Exactive mass spectrometer (Thermo Scientific). The MaxQuant software suite was used for protein identifications and LFQ (35). Protein intensities were compared using a two-sided *t* test and correcting for multiple testing by controlling for FDR at 5% using the Benjamini–Hochberg method (36). Details are provided in *SI Materials and Methods*.

**EsxG–EsxH Antibody Production and Western Blotting.** A His-tagged EsxG–EsxH fusion construct (74) was produced in *Escherichia coli* as described (19) and was used to immunize rabbits. Rabbit polyclonal serum was used in Western blotting.

**Mice and Infections.** Mouse studies were performed in accordance with National Institutes of Health guidelines (75), and all work was approved by the Albert Einstein College of Medicine Institutional Animal Care and Use Committee (Protocol #20120114). Female C57BL/6 and SCID mice were from the National Cancer Institute, and female CBA/J mice and B6.129S7-*Rag1*$^{tm1Mom}$/J (*RAG1*$^{-/-}$) mice were from Jackson Laboratories. Mycobacterial strains were grown in 7H9 medium with antibiotics as appropriate. For all infections, bacteria were washed in PBS-T and were sonicated. For i.v. infections, mice were injected via the lateral tail vein with the indicated doses of bacteria in 200 μL PBS-T. The actual dose delivered was determined by serial dilution and plating. For aerosol infections, the bacterial suspension also contained 0.04% antifoam Y-30 emulsion (Sigma) and was targeted to deliver a dose of ∼50–150 cfu per lung. Mice from each infection group were killed 24 h after aerosol exposure, and lung homogenates were plated to determine initial bacterial numbers delivered per strain. Bacterial burdens in lungs and spleen were determined by plating organ homogenates, prepared and diluted in PBS-T, from three or four mice per infection group onto appropriate medium. Details are provided in *SI Materials and Methods*.

**Statistical Analysis.** Differences between groups were analyzed by Student's *t* test. A *P* value ≤0.05 was considered statistically significant. Survival curves were compared with the log-rank (Mantel–Cox) test using GraphPad Prism for Windows (GraphPad Software). Statistical comparisons of protein intensities in CF samples were performed as described in *SI Materials and Methods*.

**ACKNOWLEDGMENTS.** We thank Bing Chen, Mei Chen, and John Kim for assistance with mouse infections; Annie Dai for phage preparation; Colin Ratledge for providing mycobactins; Brian Weinrick for mutant verification by whole genome sequencing; Michelle Larsen and Anthony Orth for sharing constructs from the Genomics Institute of the Novartis Research Foundation phasmid collection; Katherine Moccia and Eva Yang for assistance with strain generation and verification; and members of the W.R.J. and J.A.P. laboratories for numerous helpful discussions. This work was supported by NIH Grants AI26170 and AI098925 (to W.R.J.) and T32GM007288 for support of C.A.K. at the Albert Einstein College of Medicine; and NIH Grant AI087682 and funds from the New York University School of Medicine (to J.A.P.).

1. Stoop EJ, Bitter W, van der Sar AM (2012) Tubercle bacilli rely on a type VII army for pathogenicity. *Trends Microbiol* 20(10):477–484.
2. van der Woude AD, Luirink J, Bitter W (2013) Getting across the cell envelope: Mycobacterial protein secretion. *Curr Top Microbiol Immunol* 374:109–134.
3. Bitter W, et al. (2009) Systematic genetic nomenclature for type VII secretion systems. *PLoS Pathog* 5(10):e1000507.
4. Hsu T, et al. (2003) The primary mechanism of attenuation of bacillus Calmette-Guerin is a loss of secreted lytic function required for invasion of lung interstitial tissue. *Proc Natl Acad Sci USA* 100(21):12420–12425.
5. Lewis KN, et al. (2003) Deletion of RD1 from Mycobacterium tuberculosis mimics bacille Calmette-Guérin attenuation. *J Infect Dis* 187(1):117–123.
6. Pym AS, Brodin P, Brosch R, Huerre M, Cole ST (2002) Loss of RD1 contributed to the attenuation of the live tuberculosis vaccines Mycobacterium bovis BCG and Mycobacterium microti. *Mol Microbiol* 46(3):709–717.
7. Abdallah AM, et al. (2007) Type VII secretion–mycobacteria show the way. *Nat Rev Microbiol* 5(11):883–891.
8. Champion PA, Cox JS (2007) Protein secretion systems in Mycobacteria. *Cell Microbiol* 9(6):1376–1384.
9. Stanley SA, Cox JS (2013) Host-pathogen interactions during Mycobacterium tuberculosis infections. *Curr Top Microbiol Immunol* 374:211–241.
10. Rodriguez GM, Voskuil MI, Gold B, Schoolnik GK, Smith I (2002) ideR, An essential gene in mycobacterium tuberculosis: Role of IdeR in iron-dependent gene expression, iron metabolism, and oxidative stress response. *Infect Immun* 70(7):3371–3381.
11. Serafini A, Boldrin F, Palù G, Manganelli R (2009) Characterization of a Mycobacterium tuberculosis ESX-3 conditional mutant: Essentiality and rescue by iron and zinc. *J Bacteriol* 191(20):6340–6344.
12. Siegrist MS, et al. (2014) Mycobacterial Esx-3 requires multiple components for iron acquisition. *MBio* 5(3):e01073.
13. Siegrist MS, et al. (2009) Mycobacterial Esx-3 is required for mycobactin-mediated iron acquisition. *Proc Natl Acad Sci USA* 106(44):18792–18797.
14. Sweeney KA, et al. (2011) A recombinant Mycobacterium smegmatis induces potent bactericidal immunity against Mycobacterium tuberculosis. *Nat Med* 17(10):1261–1268.
15. Ilghari D, et al. (2011) Solution structure of the Mycobacterium tuberculosis EsxG·EsxH complex: Functional implications and comparisons with other M. tuberculosis Esx family complexes. *J Biol Chem* 286(34):29993–30002.

16. Billeskov R, Vingsbo-Lundberg C, Andersen P, Dietrich J (2007) Induction of CD8 T cells against a novel epitope in TB10.4: Correlation with mycobacterial virulence and the presence of a functional region of difference-1. *J Immunol* 179(6):3973–3981.
17. Hervas-Stubbs S, et al. (2006) High frequency of CD4+ T cells specific for the TB10.4 protein correlates with protection against Mycobacterium tuberculosis infection. *Infect Immun* 74(6):3396–3407.
18. Skjot RL, et al. (2002) Epitope mapping of the immunodominant antigen TB10.4 and the two homologous proteins TB10.3 and TB12.9, which constitute a subfamily of the esat-6 gene family. *Infect Immun* 70(10):5446–5453.
19. Mehra A, et al. (2013) Mycobacterium tuberculosis type VII secreted effector EsxH targets host ESCRT to impair trafficking. *PLoS Pathog* 9(10):e1003734.
20. Jones CM, Niederweis M (2011) Mycobacterium tuberculosis can utilize heme as an iron source. *J Bacteriol* 193(7):1767–1770.
21. Tullius MV, et al. (2011) Discovery and characterization of a unique mycobacterial heme acquisition system. *Proc Natl Acad Sci USA* 108(12):5051–5056.
22. Abdallah AM, et al. (2009) PPE and PE_PGRS proteins of Mycobacterium marinum are transported via the type VII secretion system ESX-5. *Mol Microbiol* 73(3):329–340.
23. McMahon MD, Rush JS, Thomas MG (2012) Analyses of MbtB, MbtE, and MbtF suggest revisions to the mycobactin biosynthesis pathway in Mycobacterium tuberculosis. *J Bacteriol* 194(11):2809–2818.
24. Jain P, et al. (2012) φ(2)GFP10, a high-intensity fluorophage, enables detection and rapid drug susceptibility testing of Mycobacterium tuberculosis directly from sputum samples. *J Clin Microbiol* 50(4):1362–1369.
25. Sambandamurthy VK, et al. (2006) Mycobacterium tuberculosis DeltaRD1 DeltapanCD: A safe and limited replicating mutant strain that protects immunocompetent and immunocompromised mice against experimental tuberculosis. *Vaccine* 24(37-39): 6309–6320.
26. De Voss JJ, et al. (2000) The salicylate-derived mycobactin siderophores of Mycobacterium tuberculosis are essential for growth in macrophages. *Proc Natl Acad Sci USA* 97(3):1252–1257.
27. Tullius MV, Harth G, Maslesa-Galic S, Dillon BJ, Horwitz MA (2008) A Replication-Limited Recombinant Mycobacterium bovis BCG vaccine against tuberculosis designed for human immunodeficiency virus-positive persons is safer and more efficacious than BCG. *Infect Immun* 76(11):5200–5214.
28. Jones CM, et al. (2014) Self-poisoning of Mycobacterium tuberculosis by interrupting siderophore recycling. *Proc Natl Acad Sci USA* 111(5):1945–1950.
29. Malo D, et al. (1994) Haplotype mapping and sequence analysis of the mouse Nramp gene predict susceptibility to infection with intracellular parasites. *Genomics* 23(1): 51–61.
30. Forbes JR, Gros P (2001) Divalent-metal transport by NRAMP proteins at the interface of host-pathogen interactions. *Trends Microbiol* 9(8):397–403.
31. Bellamy R (1999) The natural resistance-associated macrophage protein and susceptibility to intracellular pathogens. *Microbes Infect* 1(1):23–27.
32. Corna G, et al. (2010) Polarization dictates iron handling by inflammatory and alternatively activated macrophages. *Haematologica* 95(11):1814–1822.
33. Recalcati S, et al. (2010) Differential regulation of iron homeostasis during human macrophage polarized activation. *Eur J Immunol* 40(3):824–835.
34. Sierra-Filardi E, Vega MA, Sánchez-Mateos P, Corbí AL, Puig-Kröger A (2010) Heme Oxygenase-1 expression in M-CSF-polarized M2 macrophages contributes to LPS-induced IL-10 release. *Immunobiology* 215(9-10):788–795.
35. Cox J, et al. (2014) Accurate proteome-wide label-free quantification by delayed normalization and maximal peptide ratio extraction, termed MaxLFQ. *Mol Cell Proteomics* 13(9):2513–2526.
36. Benjamini Y, Hochberg Y (1995) Controlling the false discovery rate: A practical and powerful approach to multiple testing. *J R Stat Soc, B* 57(1):289–300.
37. Fortune SM, et al. (2005) Mutually dependent secretion of proteins required for mycobacterial virulence. *Proc Natl Acad Sci USA* 102(30):10676–10681.
38. Målen H, Berven FS, Fladmark KE, Wiker HG (2007) Comprehensive analysis of exported proteins from Mycobacterium tuberculosis H37Rv. *Proteomics* 7(10):1702–1718.
39. Houben EN, Korotkov KV, Bitter W (2014) Take five - Type VII secretion systems of Mycobacteria. *Biochim Biophys Acta* 1843(8):1707–1716.
40. Simeone R, Bottai D, Brosch R (2009) ESX/type VII secretion systems and their role in host-pathogen interaction. *Curr Opin Microbiol* 12(1):4–10.
41. Simeone R, Bottai D, Frigui W, Majlessi L, Brosch R (2015) ESX/type VII secretion systems of mycobacteria: Insights into evolution, pathogenicity and protection. *Tuberculosis (Edinb)* 95:5150–5154.
42. Cassat JE, Skaar EP (2013) Iron in infection and immunity. *Cell Host Microbe* 13(5): 509–519.
43. Neyrolles O, Wolschendorf F, Mitra A, Niederweis M (2015) Mycobacteria, metals, and the macrophage. *Immunol Rev* 264(1):249–263.
44. Reddy PV, et al. (2013) Disruption of mycobactin biosynthesis leads to attenuation of Mycobacterium tuberculosis for growth and virulence. *J Infect Dis* 208(8):1255–1265.
45. Madigan CA, et al. (2015) Lipidomic analysis links mycobactin synthase K to iron uptake and virulence in M. tuberculosis. *PLoS Pathog* 11(3):e1004792.
46. Wells RM, et al. (2013) Discovery of a siderophore export system essential for virulence of Mycobacterium tuberculosis. *PLoS Pathog* 9(1):e1003120.
47. Vidal S, et al. (1995) The Ity/Lsh/Bcg locus: Natural resistance to infection with intracellular parasites is abrogated by disruption of the Nramp1 gene. *J Exp Med* 182(3): 655–666.
48. Medina E, North RJ (1996) Evidence inconsistent with a role for the Bcg gene (Nramp1) in resistance of mice to infection with virulent Mycobacterium tuberculosis. *J Exp Med* 183(3):1045–1051.
49. North RJ, LaCourse R, Ryan L, Gros P (1999) Consequence of Nramp1 deletion to Mycobacterium tuberculosis infection in mice. *Infect Immun* 67(11):5811–5814.
50. Bellamy R, et al. (1998) Variations in the NRAMP1 gene and susceptibility to tuberculosis in West Africans. *N Engl J Med* 338(10):640–644.
51. Li HT, Zhang TT, Zhou YQ, Huang QH, Huang J (2006) SLC11A1 (formerly NRAMP1) gene polymorphisms and tuberculosis susceptibility: A meta-analysis. *Int J Tuberc Lung Dis* (1):3–12.
52. Beamer GL, Cyktor J, Carruthers B, Turner J (2011) H-2 alleles contribute to antigen 85-specific interferon-gamma responses during Mycobacterium tuberculosis infection. *Cell Immunol* 271(1):53–61.
53. Beamer GL, et al. (2008) Interleukin-10 promotes Mycobacterium tuberculosis disease progression in CBA/J mice. *J Immunol* 181(8):5545–5550.
54. Arbing MA, et al. (2013) Heterologous expression of mycobacterial Esx complexes in Escherichia coli for structural studies is facilitated by the use of maltose binding protein fusions. *PLoS One* 8(11):e81753.
55. Brodin P, et al. (2006) Dissection of ESAT-6 system 1 of Mycobacterium tuberculosis and impact on immunogenicity and virulence. *Infect Immun* 74(1):88–98.
56. Stanley SA, Raghavan S, Hwang WW, Cox JS (2003) Acute infection and macrophage subversion by Mycobacterium tuberculosis require a specialized secretion system. *Proc Natl Acad Sci USA* 100(22):13001–13006.
57. Rosenberg OS, et al. (2015) Substrates Control Multimerization and Activation of the Multi-Domain ATPase Motor of Type VII Secretion. *Cell* 161(3):501–512.
58. Daleke MH, et al. (2012) General secretion signal for the mycobacterial type VII secretion pathway. *Proc Natl Acad Sci USA* 109(28):11342–11347.
59. Ekiert DC, Cox JS (2014) Structure of a PE-PPE-EspG complex from Mycobacterium tuberculosis reveals molecular specificity of ESX protein secretion. *Proc Natl Acad Sci USA* 111(41):14758–14763.
60. Gey van Pittius NC, et al. (2006) Evolution and expansion of the Mycobacterium tuberculosis PE and PPE multigene families and their association with the duplication of the ESAT-6 (esx) gene cluster regions. *BMC Evol Biol* 6:95.
61. Tiwari BM, Kannan N, Vemu L, Raghunand TR (2012) The Mycobacterium tuberculosis PE proteins Rv0285 and Rv1386 modulate innate immunity and mediate bacillary survival in macrophages. *PLoS One* 7(12):e51686.
62. Maciag A, et al. (2007) Global analysis of the Mycobacterium tuberculosis Zur (FurB) regulon. *J Bacteriol* 189(3):730–740.
63. van Dam JC, Schaap PJ, Martins dos Santos VA, Suárez-Diez M (2014) Integration of heterogeneous molecular networks to unravel gene-regulation in Mycobacterium tuberculosis. *BMC Syst Biol* 8:111.
64. Betts JC, Lukey PT, Robb LC, McAdam RA, Duncan K (2002) Evaluation of a nutrient starvation model of Mycobacterium tuberculosis persistence by gene and protein expression profiling. *Mol Microbiol* 43(3):717–731.
65. Demangel C, et al. (2004) Cell envelope protein PPE68 contributes to Mycobacterium tuberculosis RD1 immunogenicity independently of a 10-kilodalton culture filtrate protein and ESAT-6. *Infect Immun* 72(4):2170–2176.
66. Bottai D, et al. (2012) Disruption of the ESX-5 system of Mycobacterium tuberculosis causes loss of PPE protein secretion, reduction of cell wall integrity and strong attenuation. *Mol Microbiol* 83(6):1195–1209.
67. Houben EN, et al. (2012) Composition of the type VII secretion system membrane complex. *Mol Microbiol* 86(2):472–484.
68. Bardarov S, et al. (2002) Specialized transduction: An efficient method for generating marked and unmarked targeted gene disruptions in Mycobacterium tuberculosis, M. bovis BCG and M. smegmatis. *Microbiology* 148(Pt 10):3007–3017.
69. Jain P, et al. (2014) Specialized transduction designed for precise high-throughput unmarked deletions in Mycobacterium tuberculosis. *MBio* 5(3):e01245–14.
70. Madigan CA, et al. (2012) Lipidomic discovery of deoxysiderophores reveals a revised mycobactin biosynthesis pathway in Mycobacterium tuberculosis. *Proc Natl Acad Sci USA* 109(4):1257–1262.
71. Prados-Rosales R, et al. (2014) Role for Mycobacterium tuberculosis membrane vesicles in iron acquisition. *J Bacteriol* 196(6):1250–1256.
72. Wong KW, Jacobs WR, Jr (2013) Mycobacterium tuberculosis exploits human interferon γ to stimulate macrophage extracellular trap formation and necrosis. *J Infect Dis* 208(1):109–119.
73. Vogt G, Nathan C (2011) In vitro differentiation of human macrophages with enhanced antimycobacterial activity. *J Clin Invest* 121(10):3889–3901.
74. Callahan B, et al. (2010) Conservation of structure and protein-protein interactions mediated by the secreted mycobacterial proteins EsxA, EsxB, and EspA. *J Bacteriol* 192(1):326–335.
75. Committee on Care and Use of Laboratory Animals (1996) *Guide for the Care and Use of Laboratory Animals* (Natl Inst Health, Bethesda), DHHS Publ No (NIH) 85-23.
76. Tufariello JM, et al. (2014) Enhanced specialized transduction using recombineering in Mycobacterium tuberculosis. *MBio* 5(3):e01179–14.
77. Larsen MH, Biermann K, Tandberg S, Hsu T, Jacobs WR (2007) Genetic manipulation of Mycobacterium tuberculosis. *Curr Protoc Microbiol* 6:(A):10A.2.1–10A.2.21.
78. Braunstein M, et al. (2000) Identification of genes encoding exported Mycobacterium tuberculosis proteins using a Tn552'phoA in vitro transposition system. *J Bacteriol* 182(10):2732–2740.
79. Stover CK, et al. (1991) New use of BCG for recombinant vaccines. *Nature* 351(6326): 456–460.